Disentangling the Role of Heterogeneity and Hyperedge Overlap in Explosive Contagion on Higher-Order Networks

Federico Malizia,[1,*] Andrés Guzmán,[1] Iacopo Iacopini,[1,2] and István Z. Kiss[1,3,†]

[1]*Network Science Institute, Northeastern University London, London E1W 1LP, United Kingdom*
[2]*Department of Physics, Northeastern University, Boston, MA 02115, USA*
[3]*Department of Mathematics, Northeastern University, Boston, MA 02115, USA*

(Dated: October 7, 2025)

We introduce group-based compartmental modeling (GBCM), a mean-field framework for irreversible contagion in higher-order networks that captures structural heterogeneity and correlations across group sizes. Validated through numerical simulations, GBCM analytically disentangles the role of each interaction order to the global epidemic dynamics, revealing how heterogeneity and inter-order correlations jointly shape the onset of outbreaks and the emergence of explosive dynamics. Crucially, we show that inter-order correlations drive the system along distinct pathways to explosive contagion—emerging universally across both irreversible and reversible spreading processes.

The propagation of contagions and behaviors in complex systems is often driven by interactions that involve groups of more than two individuals [1–3]. Such higher-order mechanisms can generate striking collective phenomena, including explosive transitions and multistability across diverse systems [4–6]. The organization of group interactions—through both degree distributions and their microscopic arrangement—plays a decisive role in shaping system behavior [7–12], with hubs in higher-order structures exerting a significant influence on epidemic onset and evolution [13, 14]. Yet, developing analytically tractable models that capture both structural correlations and degree heterogeneity remains a fundamental challenge.

In this Letter, we develop a group-based mean-field framework for the Susceptible–Infected–Recovered (SIR) dynamics on higher-order networks. Our model captures two key structural features: heterogeneity in hyperdegree distributions and the *inter-order hyperedge overlap* [15], which quantifies correlations across interaction orders. By deriving the epidemic threshold and disentangling the roles of two- and three-body interactions, we show how these features jointly shape epidemic onset. We find that strong heterogeneity can trigger explosive contagion, while overlap modulates the early-stage activation of higher-order spreading pathways. These predictions, validated by Gillespie simulations on synthetic and empirical hypergraphs, also extend to SIS dynamics. Altogether, our results reveal the structural and dynamical mechanisms underlying abrupt contagion transitions and provide a unifying framework for spreading processes in complex systems.

Modeling higher-order interactions.—We model a system with higher-order interactions as a hypergraph $H = (\mathcal{N}, \mathcal{E})$, where $\mathcal{N}$ is the set of $N = |\mathcal{N}|$ nodes and $\mathcal{E}$ the set of $E = |\mathcal{E}|$ hyperedges (groups of nodes). Each hyperedge $e \in \mathcal{E}$, a subset of $\mathcal{N}$, has order $m = |e| - 1$, with $m = 1$ for pairwise links, $m = 2$ for three-body interactions, etc. We denote by $\mathcal{E}_m$ the set of m-hyperedges, and by k_m the generalized degree (or k-hyperdegree), i.e., the number of m-hyperedges attached to a node [16]. Let $P(k_m)$ denote the m-hyperdegree distribution, with first two moments $\langle k_m \rangle$ and $\langle k_m^2 \rangle$ capturing mean connectivity and heterogeneity. These distributions, however, do not capture the microscopic arrangement of hyperedges or correlations across orders. To quantify such correlations we compare a structure to the inclusion property of simplicial complexes [17]. Let $\mathcal{F}(\mathcal{E}_n)$ denote the set of m-cliques contained in n-hyperedges. For two orders $m < n$, the *inter-order hyperedge overlap* is [15]

$$\alpha_{m,n} = \frac{\left|\mathcal{E}_m \cap \mathcal{F}(\mathcal{E}_n)\right|}{\left|\mathcal{F}(\mathcal{E}_n)\right|}, \tag{1}$$

where the numerator counts m-cliques in n-hyperedges that are also m-hyperedges, normalized by the total number of such cliques. Thus $\alpha_{m,n} \in [0, 1]$, with $\alpha_{m,n} = 0$ for no overlap and $\alpha_{m,n} = 1$ when all m-cliques in n-hyperedges are also m-hyperedges. By definition, $\alpha_{m,n} = 0$ for $m > n$. Empirical higher-order networks display a broad range of $\alpha_{m,n}$ values, as shown in Sec.I of the Supplemental Material (SM) [18].

Group-based compartmental modeling.—To understand how correlations between different orders of interactions affect the onset and outcome of outbreaks, we propose a mathematical framework that explicitly includes the inter-order overlap of Eq. (1) as a free parameter. Building on the edge-based compartmental modeling approach for SIR on networked systems [19–22], we generalize it to capture infection within groups of arbitrary order $m = 1, 2, \ldots, M$. Each order m has infection rate β_m, describing the rate at which a susceptible node is infected through a "contagious" m-hyperedge, i.e., one where all other m nodes are infectious. The recovery rate is μ, and recovered nodes cannot be reinfected. We refer to this framework as group-based compartmental modeling (GBCM). It relies on two key quantities for a test node u: $\theta_m(t)$, the probability that u has not been infected by a random infectious m-hyperedge at time t; and $\Phi_m^{(s,i)}(t)$, the

* maliziaf@ceu.edu
† istvan.kiss@nulondon.ac.uk

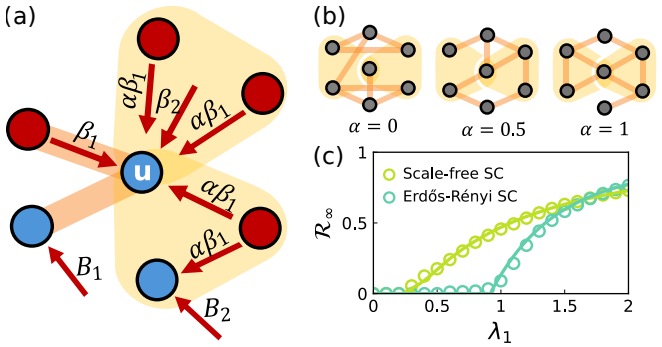

FIG. 1. **Group-based compartmental modeling.** (a) Graphical representation of the model for $M = 2$. A test node u is connected to four infectious (red) and two susceptible (blue) nodes via two 1-hyperedges and two 2-hyperedges. Arrows show the different channels of infection through the rate parameters in Eq. (4). (b) Motifs representing three values of inter-order hyperedge overlap α: 0, 0.5, and 1. (c) Final epidemic size ($\mathcal{R}_\infty$) as a function of infectivity λ_1, with $\lambda_2 = 3$. Model results (lines) are compared with Gillespie simulations (markers) on Scale-Free and an Erdős-Rényi simplicial complexes, respectively with 2,000 and 10,000 nodes (see characteristics in Table I).

probability that u is susceptible and part of an m-hyperedge with s susceptible and i infected nodes. With these, $\theta_m(t) = \sum_{(s,i)\in\Omega} \Phi_m^{(s,i)}(t)$, where $\Omega = \{(s,i) \mid 0 \le s+i \le m\}$. The $\Phi_m^{(s,i)}$ describe epidemic progression within m-hyperedges, from fully susceptible to fully infected, and their dynamics depend on $\alpha_{m,n}$, which couples contagion across orders. For simplicity we omit time dependence henceforth. The evolution of θ_m follows $\dot{\theta}_m = -\beta_m \Phi_m^{(0,m)}$. To account for the distribution of m-hyperedges around a node, we use probability generating functions (PGFs) [23, 24]. The PGF of order m is

$$G_m(\theta_m) = \sum_{k_m=0}^{\infty} P(k_m)\theta_m^{k_m}. \tag{2}$$

Assuming independence among orders, the fraction of susceptibles is $\langle S\rangle = \prod_{m=1}^{M} G_m(\theta_m)$. This formalism naturally suits SIR, where irreversibility permits a mapping to bond percolation [23, 25]. Unlike classical dyadic SIR, it disentangles the contribution of each order. By differentiating $\langle S\rangle$, separating the contributions by order of interaction, and incorporating a recovery term, we obtain

$$\dot{\langle I_m\rangle} = -G'_m(\theta_m)\dot{\theta}_m \prod_{n\neq m} G_n(\theta_n) - \mu\langle I_m\rangle. \tag{3}$$

Finally, the total densities of infected and recovered populations at time t are, respectively, $\langle I\rangle = \sum_{m=1}^{M}\langle I_m\rangle$ and $\langle R\rangle = 1 - \langle S\rangle - \langle I\rangle$. To fully appreciate and explicitly show the components of the GBCM, we restrict our analysis to interactions up to order $m \le 2$ (see Appendix for the general formulation up to any M). In this case, the inter-order hyperedge overlap reduces to $\alpha_{1,2} \equiv \alpha$, which quantifies the extent to which 2-body interactions are contained within 3-body interactions. The formalism thus captures both the independent contributions of different orders and their interplay through α, as illustrated in Fig. 1(a). In addition, Fig.1(b) illustrates three simple scenario corresponding to different values of the inter-order hyperedge overlap α. To further simplify the notation, we define $G(\theta_1) \equiv G_1(\theta_1)$, $H(\theta_2) \equiv G_2(\theta_2)$, and similarly $\phi_S \equiv \Phi_1^{(1,0)}$, $\phi_I \equiv \Phi_1^{(0,1)}$, $\phi_{SI} \equiv \Phi_2^{(1,1)}$, and $\phi_{II} \equiv \Phi_2^{(0,2)}$. Under these assumptions, the resulting system of coupled equations for the GBCM with $M = 2$ is given by

$$\begin{aligned}
\dot{\theta_1} &= -\beta_1\phi_I; \quad \dot{\theta_2} = -\beta_2\phi_{II},\\
\dot{\phi_I} &= B_1\phi_S - (\beta_1+\mu)\phi_I - 2\alpha\beta_1\phi_{II},\\
\dot{\phi_{SI}} &= 2B_2\phi_{SS} - (B_2+\mu)\phi_{SI} - 2\alpha\beta_1\phi_{SI},\\
\dot{\phi_{II}} &= B_2\phi_{SI} - (\beta_2+2\mu)\phi_{II} + \alpha\beta_1(\phi_{SI} - 2\phi_{II}),
\end{aligned} \tag{4}$$

where $\phi_S = G'(\theta_1)H(\theta_2)/\langle k_1\rangle$ and $\phi_{SS} = (G(\theta_1)H'(\theta_2)/\langle k_2\rangle)^2$ (see Appendix for their detailed derivation), with $\langle k_m\rangle = \sum_{k_m} k_m P(k_m)$, corresponding to the first derivative of the PGF, defined in Eq. (2), when $\theta_m(t) = 1$. Moreover, B_1 and B_2 in Eq. (4) represent the rate of infection from external 1- and 2-hyperedges, respectively (see Appendix for their detailed expressions). Notice how α appears explicitly in the equations for the evolution of ϕ_I, ϕ_{SI} and ϕ_{II}. In particular, the term $-2\alpha\beta_1\phi_{SI}$ accounts for the potential infections coming from pairwise interactions nested within 2-hyperedges—with similar arguments for the other terms involving α. This formulation allows us to incorporate dynamical correlations arising from the embedding of 1- within 2-hyperedges, without system closures tailored to specific microscopic configurations. Henceforth, we use the rescaled infectivity parameters $\lambda_1 = \langle k_1\rangle\beta_1/\mu$ and $\lambda_2 = \langle k_2\rangle\beta_2/\mu$ [5]. We validate our approach by comparing the final epidemic size ($\mathcal{R}_\infty$) predicted by the GBCM with averages from 500 Gillespie simulations over different higher-order networks with $\alpha = 1$ (i.e., simplicial complexes), see Fig. 1(c). The structures used to run simulations exhibit Scale-Free (SF) and Erdős-Rényi-like (ER) hyperdegree distributions at both orders $m = 1$ and $m = 2$, with their characteristics summarized in Table I. The ER and SF simplicial complexes were generated following [5] and [26], respectively. In both cases, the GBCM predictions closely match the simulations, demonstrating the model's ability to capture the dynamics of higher-order systems.

The role of inter-order hyperedge overlap.— Here, we

Higher-order networks	$\langle k_1\rangle$	$\langle k_1^2\rangle$	$\langle k_2\rangle$	$\langle k_2^2\rangle$
Regular	6.00	42.00	1.00	2.00
Erdős-Rényi	11.83	169.51	2.90	14.30
Scale-Free	11.98	649.76	9.00	610.10

TABLE I. Characteristics of different higher-order networks considered in the study, where $\langle k_1\rangle$ and $\langle k_2\rangle$ denote the mean hyperdegree for pairwise and higher-order interactions, respectively, while $\langle k_1^2\rangle$ and $\langle k_2^2\rangle$ are the second moments of the hyperdegree distributions.

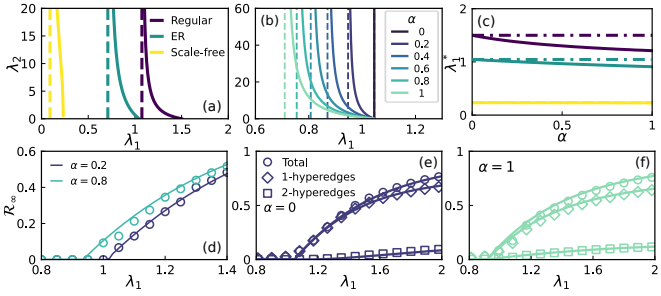

FIG. 2. **The role of inter-order hyperedge overlap.** Epidemic thresholds in the (λ_1, λ_2) plane predicted by the GBCM, Eq. (15): (a) for simplicial complexes ($\alpha = 1$) in Table I; (b) for Erdős-Rényi hypergraphs with different α values. (c) Epidemic threshold λ_1^* as a function of α (fixed $\lambda_2 = 3$) for the three classes of hypergraphs. (d-f) Comparison of the final epidemic size $\mathcal{R}_\infty$ from the GBCM model (lines) and simulations (markers) on ER hypergraphs with $N = 10{,}000$ nodes, for different α. In (d) we show $\mathcal{R}_\infty$ against λ_1 for different overlap values. In (e) and (f), we consider the extreme cases $\alpha = 0$ and $\alpha = 1$ and show $\mathcal{R}_\infty$ disaggregated by contributions from 1- and 2-hyperedges. In all cases, $\mu = 1$.

study the stability of the disease-free state of Eqs. (4) by evaluating the Jacobian at $(\theta_1, \theta_2, \phi_I, \phi_{SI}, \phi_{II}) = (1, 1, 0, 0, 0)$. Despite the model's complexity, we find an analytical expression for the epidemic threshold, revealing its explicit dependence on the interplay between structural overlap and hyperdegree heterogeneity. This maps the critical relationship between λ_1 and λ_2 at the epidemic threshold (see Appendix for details). Figure 2(a) shows the epidemic threshold in the (λ_1, λ_2) plane for simplicial complexes ($\alpha = 1$) with three heterogeneity levels (Table I). Dashed lines indicate $\lambda_1 = \lambda_1^c$ where $\lambda_2 \to \infty$, showing no outbreak is possible if $\lambda_1 \leq \lambda_1^c$ regardless of λ_2; thus pairwise transmission dominates. Fig. 2(b) shows ER hypergraphs with varying overlap, where increasing α consistently lowers the epidemic threshold. To explore the threshold's α-dependency, we rearrange it as a third-order polynomial in λ_1. Its solution λ_1^*, the critical λ_1 for epidemic onset, can be approximated using an asymptotic expansion for small α (see Sec.II of the SM for details), yielding

$$\lambda_1^* \approx \frac{\langle k_1\rangle^2}{\Delta_1} - \alpha\lambda_2 \frac{2\langle k_1\rangle^5\langle k_2\rangle}{\Delta_1^3\left(2\langle k_2\rangle + \lambda_2\right)}, \tag{5}$$

where $\Delta_m = \Pi_m - \langle k_m\rangle$ and $\Pi_m = \langle k_m^2\rangle - \langle k_m\rangle = \sum_{k_m} k_m(k_m - 1)P(k_m)$. The latter expression represents the second derivative of the PGF evaluated at $\theta_m(t) = 1$. It is worth noting that Δ_m represents the difference between the second and first derivatives of the PGF at $\theta_m(t) = 1$. This result highlights that stronger inter-order correlations ($\alpha > 0$) increase the system's susceptibility to outbreaks. Furthermore, when $\alpha \neq 0$, λ_1^* depends on the strength of higher-order interactions (λ_2), in line with with recent findings [27, 28]. Additionally, Eq. (5) demonstrates that greater heterogeneity in the pairwise degree distribution (via Δ_1) reduces the influence of higher-order interactions on λ_1^*. Fig. 2(c) shows the dependence of the exact epidemic threshold λ_1^* on α, numerically evaluated from the Jacobian matrix of the system in Eq.(4), with $\lambda_2 = 3$; the dashed-dotted line denotes the $\alpha = 0$ baseline.

We next examine the final epidemic size. Figure 2(d-f) compares GBCM predictions with averages from 500 simulations on ER hypergraphs with varying α. To generate a continuous spectrum of higher-order networks with overlap $\alpha \in [0, 1]$, we rewire the 1-hyperedge layer of the ER simplicial complex while preserving its 1-hyperdegree distribution and 2-hyperedge structure (see Sec. IV of the SM for details). Figure 2(d) confirms that the GBCM accurately predicts the epidemic threshold, which depends on inter-order overlap: increasing α anticipates epidemic onset. Figures 2(e)-(f) disentangle pairwise and higher-order contagion contributions to final epidemic size for $\alpha = 0$ and $\alpha = 1$, respectively. For $\alpha = 0$, three-body transmission requires infected node buildup to activate. For $\alpha = 1$, both contagion modes activate simultaneously at λ_1^*, as predicted by Eq. (15).

High heterogeneity of group interactions leads to explosive phenomena.—We systematically analyze how heterogeneity in hyperdegree distributions affects epidemic dynamics, examining both final epidemic size and temporal evolution. We consider three synthetic hypergraphs ($N = 10{,}000$ nodes) with uncorrelated negative binomial hyperdegree distributions [29], independently tuning 2-hyperdegree variance while fixing mean degrees. The mean pairwise degree is $\langle k_1\rangle \approx 12$ with $\langle k_1^2\rangle = 327$. For three-body interactions, $\langle k_2\rangle \approx 9$ with heterogeneity levels $\Delta_2 \approx [100, 250, 600]$, measuring the difference between second and first PGF derivatives at $\theta_2(t) = 1$ (see Sec.V of the SM). All cases have zero inter-order overlap ($\alpha = 0$). Figure 3(a) shows final epidemic size versus λ_1 for $\lambda_2 = 6$ ($\beta_2 \approx 0.66$) across three heterogeneity levels. GBCM predictions match averages over 500 simulations across all levels. Increasing Δ_2 produces more abrupt epidemic transitions. Figures 3(b)-(c) decompose 1- and 2-hyperedge contributions to final epidemic size for $\Delta_2 \approx 250$ and $\Delta_2 \approx 600$, respectively. Both show double transitions due to $\alpha = 0$. At λ_1^* (epidemic threshold from Eq. (15)), the system exhibits continuous transitions driven by 1-hyperedges. Figure 3(b) shows a secondary increase at λ_1, marking higher-order contagion onset. At higher heterogeneity ($\Delta_2 \approx 600$), Fig. 3(c) reveals hybrid transitions dominated by abrupt 2-hyperedge contributions. Figure 3(d) confirms that increasing Δ_2 sharpens transitions, driving explosive phenomena without inter-order overlap. In Sec.VI of the SM we provide additional evidence of explosive dynamics in empirical higher-order networks.

To better understand the mechanism leading to explosive contagion, we examine the temporal evolution of the epidemic. Fixing the pairwise infectivity at $\lambda_1 = 1$ and varying λ_2, we track the prevalence ρ over time, again decomposing the contributions to the infection from different orders via the GBCM. Figure 3(e-h) show that for low heterogeneity ($\Delta_2 \approx 100$), infections via 2-hyperedges are delayed until parwise interactions generate a critical mass of infectious nodes. For high heterogeneity ($\Delta_2 \approx 600$), shown

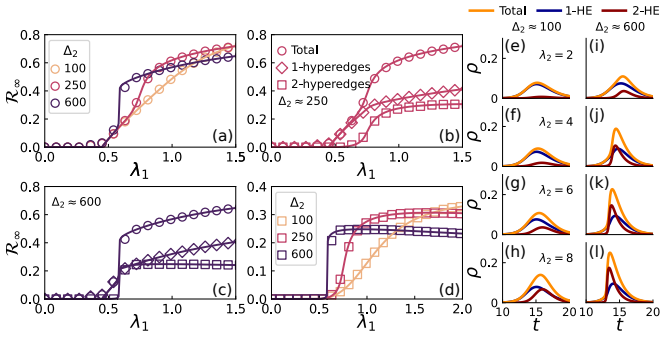

FIG. 3. **High heterogeneity of group interactions leads to explosive phenomena.** (a) Final epidemic size ($\mathcal{R}_\infty$) from GBCM predictions (solid lines) and Gillespie simulations (circles), showing excellent agreement. (b-d) Illustration of the double-transition process: (b-c) compare $\mathcal{R}_\infty$ for different heterogeneity levels in 2-hyperedges, where (c) highlights continuous transitions at λ_1^* (pairwise interactions) and abrupt jumps at $\hat{\lambda}_1$ (high heterogeneity). (d) Contribution of 2-hyperedges to $\mathcal{R}_\infty$ for increasing Δ_2, revealing sharper transitions with increasing heterogeneity. (e-l) Temporal evolution of the total prevalence ρ (orange) and contributions from pairwise (blue, 1-HE) and three-body (red, 2-HE) interactions with varying λ_2. Curves are obtained via the GBCM for hypergraphs featuring negative binomial hyperdegree distributions ($\alpha = 0$) with $\Delta_2 \approx 100$ (e-h) and $\Delta_2 \approx 600$ (i-l).

in Fig. 3(i-l), higher-order contagion rapidly amplifies epidemics, with 2-hyperedges driving the explosive growth once pairwise spreading passes a threshold.

An intuitive explanation for explosive contagion can be gained by considering the density of infected individuals through 2-hyperedges, given by $\langle \dot{I}_2 \rangle = -G(\theta_1)H'(\theta_2)\dot{\theta}_2 - \mu\langle I_2 \rangle$. Since explosive behavior occurs when $\langle \dot{I}_2 \rangle \to \infty$ at some time $\hat{t} > 0$, the condition for the critical value $\hat{\lambda}_2$ reads

$$\hat{\lambda}_2 \approx \frac{2\langle k_2 \rangle^2 \left(\langle k_1 \rangle + \alpha\lambda_1\right)}{\langle k_1 \rangle \left(\Delta_2 \hat{\phi}_{SI} + \langle k_2 \rangle(\hat{\phi}_{SI} - 1)\right)}, \tag{6}$$

where $\hat{\phi}_{SI}$ represents the critical density of ϕ_{SI} required to activate contagion via 2-hyperedges, constrained by $\epsilon \leq \hat{\phi}_{SI} \leq 1$ (see Sec.IV of the SM for the full derivation). This result shows that higher values of Δ_2 reduce the critical $\hat{\lambda}_2$, making explosive behavior more likely, whereas lower Δ_2 suppress such phenomena by increasing $\hat{\lambda}_2$. Despite the lack of an exact analytical expression for $\hat{\phi}_{SI}$, Eq. (6) provides an important explanation of the role of heterogeneity in the three-body interactions, both from a structural and dynamical viewpoint.

Inter-order hyperedge overlap modulates early-stage contributions to explosive contagion.—Having shown how hyperdegree heterogeneity triggers abrupt epidemic surges, we investigate how inter-order hyperedge overlap shapes early-stage dynamics leading to explosive behavior. We examine SF and ER hypergraphs in Table I, exploring the full range of α under two heterogeneity levels. Figures 4(a)-(b) and (d)-(e) show GBCM-predicted temporal evolution of infected densities for SF and ER cases at $\alpha = 0$ and $\alpha = 1$. As expected, high heterogeneity of SF produces

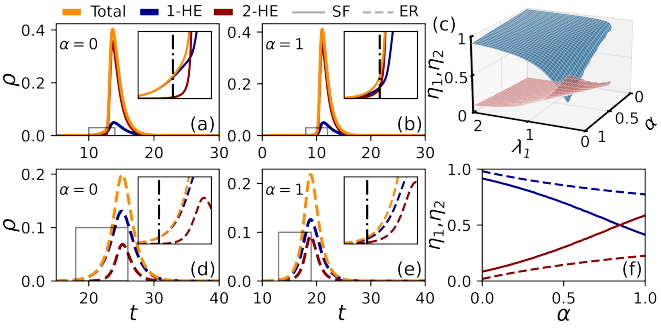

FIG. 4. **Inter-order hyperedge overlap modulates early-stage contributions to explosive contagion.** Temporal evolution of prevalence from GBCM for Scale-Free (a-b) and Erdős-Rényi (d-e) hypergraphs (see Table I), for $\lambda_2 = 15$, with $\alpha = 0$ and $\alpha = 1$. Values of λ_1 are chosen to yield $\mathcal{R}_\infty = 0.8$ in each case. Vertical lines mark the time $t^\dagger$ at which the total $\rho(t^\dagger) = 0.01$. (c) early-stage contributions η_1 (blue) and η_2 (red) evaluated at $t^\dagger$ across the (λ_1, α) space for SF hypergraphs. The same in (f) as a function of α for SF (solid lines, $\lambda_1 = 0.4$) and ER (dashed lines, $\lambda_1 = 1.6$), both at $\lambda_2 = 15$.

explosive dynamics. However, overlap effects are clear: for $\alpha = 0$, 2-hyperedge contagion activation requires critical pairwise infection density to trigger group transmission. For $\alpha = 1$, pairwise and higher-order components emerge simultaneously, suggesting overlap catalyzes early higher-order contagion activation. This behavior links to the divergence $\langle \dot{I}_2 \rangle \to \infty$ at $t = \hat{t}$, marking explosive higher-order-driven onset. For $t < \hat{t}$, spread is pairwise-driven; at $t \geq \hat{t}$, contagion becomes higher-order dominated. To quantify this tipping point empirically, we define early-stage contributions $\eta_m = \bar{\rho}_m(t^\dagger)/\sum_m \bar{\rho}_m(t^\dagger)$, where $\bar{\rho}_m(t)$ denotes cumulative infection density via m-hyperedges (ignoring recovery), evolving as $\dot{\bar{\rho}}_m = -G'_m(\theta_m)\dot{\theta}_m \prod_{n \neq m} G_n(\theta_n)$. We set $t^\dagger$ when total prevalence reaches $\rho(t^\dagger) = 0.01$, representing macroscopic contagion onset. Though $t^\dagger$ does not coincide with the singularity at $\hat{t}$, η_m provides a practical model-grounded proxy for the interaction order seeding outbreaks. Figure 4(c) shows early-stage contributions η_1 (blue) and η_2 (red) across the (λ_1, α) plane for SF hypergraphs ($\lambda_2 = 15$). While pairwise infections dominate most regions, three-body interactions contribute significantly—even dominating—at high overlap and low λ_1 (near threshold). Importantly, all regimes exhibit explosive transitions regardless of activation mechanism; overlap reshapes but does not suppress explosive contagion emergence. Figure 4(f) summarizes η_1 and η_2 versus α for SF (solid) and ER (dashed) structures. In low-heterogeneity ER, increasing α directly enhances early 2-hyperedge infections given large λ_2. In SF, overlap influence is nuanced: at high α, 1- and 2-hyperedges contribute comparably; at low α, pairwise infections dominate initially with group transmission igniting later. These findings clarify hyperedge overlap's distinct role in shaping microscopic spreading routes by regulating higher-order contagion activation timing and its contribution to explosive contagion. In Secs.VII and VIII of the SM we extend this analysis across broader parameter space and confirm the effects through Gillespie simulations, including SIS dynamics.

Conclusions.—In this Letter, we introduced a group-based mean-field framework for irreversible contagion on higher-order networks, incorporating both hyperdegree heterogeneity and inter-order correlations. Applied to two- and three-body interactions, it predicts epidemic thresholds, disentangles the contributions of each order, and explains explosive transitions arising from strong higher-order infectivity and group heterogeneity. Analytical results and Gillespie simulations show that inter-order overlap modulates the onset of higher-order contagion, shaping the microscopic pathways to explosive spreading. Although we focused on SIR dynamics for analytical tractability, the findings extend to reversible SIS processes, highlighting their generality. Extending the GBCM formalism to fully reversible dynamics remains an open challenge, as the breakdown of the percolation mapping may require approximations that compromise accuracy. Overall, our framework underscores the importance of higher-order features in contagion dynamics and provides a basis for more advanced models that incorporate structural, adaptive [30], or temporal [31, 32] effects, as well as the interplay of multiple interacting processes [33–35].

Acknowledgments.— Authors acknowledge Joel C. Miller for valuable comments.

Data availability— The data that support the findings of this Letter are openly available [36]

[1] Damon Centola and Michael Macy. Complex contagions and the weakness of long ties. *American journal of Sociology*, 113(3):702–734, 2007.

[2] Nathan O Hodas and Kristina Lerman. The simple rules of social contagion. *Scientific reports*, 4(1):4343, 2014.

[3] Federico Battiston, Giulia Cencetti, Iacopo Iacopini, Vito Latora, Maxime Lucas, Alice Patania, Jean-Gabriel Young, and Giovanni Petri. Networks beyond pairwise interactions: Structure and dynamics. *Physics reports*, 874:1–92, 2020.

[4] Federico Battiston, Enrico Amico, Alain Barrat, Ginestra Bianconi, Guilherme Ferraz de Arruda, Benedetta Franceschiello, Iacopo Iacopini, Sonia Kéfi, Vito Latora, Yamir Moreno, et al. The physics of higher-order interactions in complex systems. *Nature Physics*, 17(10):1093–1098, 2021.

[5] Iacopo Iacopini, Giovanni Petri, Alain Barrat, and Vito Latora. Simplicial models of social contagion. *Nature communications*, 10(1):2485, 2019.

[6] Per Sebastian Skardal and Alex Arenas. Higher order interactions in complex networks of phase oscillators promote abrupt synchronization switching. *Communications Physics*, 3(1):218, 2020.

[7] Guillaume St-Onge, Hanlin Sun, Antoine Allard, Laurent Hébert-Dufresne, and Ginestra Bianconi. Universal nonlinear infection kernel from heterogeneous exposure on higher-order networks. *Physical review letters*, 127(15):158301, 2021.

[8] Soumen Majhi, Matjaž Perc, and Dibakar Ghosh. Dynamics on higher-order networks: A review. *Journal of the Royal Society Interface*, 19(188):20220043, 2022.

[9] Marco Mancastroppa, Iacopo Iacopini, Giovanni Petri, and Alain Barrat. Hyper-cores promote localization and efficient seeding in higher-order processes. *Nature Communications*, 14(1):6223, 2023.

[10] Sagnik Nandy and Bhaswar B Bhattacharya. Degree heterogeneity in higher-order networks: Inference in the hypergraph β-model. *IEEE Transactions on Information Theory*, 2024.

[11] Jung-Ho Kim and K-I Goh. Higher-order components dictate higher-order contagion dynamics in hypergraphs. *Physical review letters*, 132(8):087401, 2024.

[12] Federico Malizia, Santiago Lamata-Otín, Mattia Frasca, Vito Latora, and Jesús Gómez-Gardeñes. Hyperedge overlap drives explosive transitions in systems with higher-order interactions. *Nature Communications*, 16(1):555, 2025.

[13] Nicholas W Landry and Juan G Restrepo. The effect of heterogeneity on hypergraph contagion models. *Chaos: An Interdisciplinary Journal of Nonlinear Science*, 30(10), 2020.

[14] Guillaume St-Onge, Iacopo Iacopini, Vito Latora, Alain Barrat, Giovanni Petri, Antoine Allard, and Laurent Hébert-Dufresne. Influential groups for seeding and sustaining nonlinear contagion in heterogeneous hypergraphs. *Communications Physics*, 5(1):25, 2022.

[15] Santiago Lamata-Otín, Federico Malizia, Vito Latora, Mattia Frasca, and Jesús Gómez-Gardeñes. Hyperedge overlap drives synchronizability of systems with higher-order interactions. *Physical Review E*, 111(3):034302, 2025.

[16] Owen T Courtney and Ginestra Bianconi. Generalized network structures: The configuration model and the canonical ensemble of simplicial complexes. *Physical Review E*, 93(6):062311, 2016.

[17] Allen Hatcher. *Algebraic topology*. Cambridge University Press, Cambridge, MA, 2002.

[18] See Supplemental Material (SM) at [URL] for additional figures, analysis of inter-order hyperedge overlap in real-world datasets, detailed derivations of the epidemic threshold and the condition for explosive dynamics, and further stochastic simulations of SIR and SIS processes in synthetic hypergraphs, highlighting the universal role of inter-order hyperedge overlap in shaping the pathways leading to explosive contagion. The SM includes Refs. [37–44].

[19] Romualdo Pastor-Satorras, Claudio Castellano, Piet Van Mieghem, and Alessandro Vespignani. Epidemic processes in complex networks. *Reviews of modern physics*, 87(3):925–979, 2015.

[20] István Z Kiss, Joel C Miller, Péter L Simon, et al. Mathematics of epidemics on networks. *Cham: Springer*, 598(2017):31, 2017.

[21] Joel C Miller, Anja C Slim, and Erik M Volz. Edge-based compartmental modelling for infectious disease spread. *Journal of the Royal Society Interface*, 9(70):890–906, 2012.

[22] Erik M Volz, Joel C Miller, Alison Galvani, and Lauren Ancel Meyers. Effects of heterogeneous and clustered contact patterns on infectious disease dynamics. *PLoS computational biology*, 7(6):e1002042, 2011.

[23] Mark EJ Newman. Spread of epidemic disease on networks. *Physical review E*, 66(1):016128, 2002.

[24] Joel C Miller. A primer on the use of probability generating functions in infectious disease modeling. *Infectious Disease Modelling*, 3:192–248, 2018.

[25] Eben Kenah and James M Robins. Second look at the spread of epidemics on networks. *Physical Review E—Statistical, Nonlinear, and Soft Matter Physics*, 76(3):036113, 2007.

[26] Kiriil Kovalenko, Irene Sendiña-Nadal, Nagi Khalil, Alex Dainiak, Daniil Musatov, Andrei M Raigorodskii, Karin Alfaro-Bittner, Baruch Barzel, and Stefano Boccaletti. Growing scale-free simplices. *Communications physics*, 4(1):43, 2021.

[27] Giulio Burgio, Sergio Gómez, and Alex Arenas. Triadic ap-

proximation reveals the role of interaction overlap on the spread of complex contagions on higher-order networks. *Physical Review Letters*, 132(7):077401, 2024.

[28] Federico Malizia, Luca Gallo, Mattia Frasca, István Z Kiss, Vito Latora, and Giovanni Russo. A pair-based approximation for simplicial contagion. *Chaos, Solitons & Fractals*, 199:116776, 2025.

[29] István Z Kiss, Eben Kenah, and Grzegorz A Rempała. Necessary and sufficient conditions for exact closures of epidemic equations on configuration model networks. *Journal of Mathematical Biology*, 87(2):36, 2023.

[30] Giulio Burgio, Guillaume St-Onge, and Laurent Hébert-Dufresne. Characteristic scales and adaptation in higher-order contagions. *Nature Communications*, 16(1):4589, 2025.

[31] Luca Gallo, Lucas Lacasa, Vito Latora, and Federico Battiston. Higher-order correlations reveal complex memory in temporal hypergraphs. *Nature Communications*, 15(1):4754, 2024.

[32] Iacopo Iacopini, Márton Karsai, and Alain Barrat. The temporal dynamics of group interactions in higher-order social networks. *Nature Communications*, 15(1):7391, 2024.

[33] Byungjoon Min and Maxi San Miguel. Competing contagion processes: Complex contagion triggered by simple contagion. *Scientific reports*, 8(1):10422, 2018.

[34] Maxime Lucas, Iacopo Iacopini, Thomas Robiglio, Alain Barrat, and Giovanni Petri. Simplicially driven simple contagion. *Physical Review Research*, 5(1):013201, 2023.

[35] Elsa Andres, Romualdo Pastor-Satorras, Michele Starnini, and Márton Karsai. Competition between simple and complex contagion on temporal networks. *arXiv preprint arXiv:2410.22115*, 2024.

[36] https://github.com/federicomalizia.

[37] Nicholas W. Landry, Maxime Lucas, Iacopo Iacopini, Giovanni Petri, Alice Schwarze, Alice Patania, and Leo Torres. XGI: A Python package for higher-order interaction networks. *Journal of Open Source Software*, 8(85):5162, May 2023.

[38] Piotr Sapiezynski, Arkadiusz Stopczynski, David Dreyer Lassen, and Sune Lehmann. Interaction data from the copenhagen networks study. *Scientific Data*, 6(1):315, 2019.

[39] Vsevolod Salnikov, Daniele Cassese, and Renaud Lambiotte. Simplicial complexes and complex systems. *European Journal of Physics*, 40(1):014001, 2018.

[40] Jean-Gabriel Young, Giovanni Petri, Francesco Vaccarino, and Alice Patania. Construction of and efficient sampling from the simplicial configuration model. *Physical Review E*, 96(3):032312, 2017.

[41] Konstantin Zuev, Or Eisenberg, and Dmitri Krioukov. Exponential random simplicial complexes. *Journal of Physics A: Mathematical and Theoretical*, 48(46):465002, 2015.

[42] Owen T Courtney and Ginestra Bianconi. Weighted growing simplicial complexes. *Physical Review E*, 95(6):062301, 2017.

[43] Vito Latora, Vincenzo Nicosia, and Giovanni Russo. *Complex networks: principles, methods and applications*. Cambridge University Press, 2017.

[44] Guilherme Ferraz de Arruda, Alberto Aleta, and Yamir Moreno. Contagion dynamics on higher-order networks. *Nature Reviews Physics*, 6(8):468–482, 2024.

END MATTER

Appendix A: Group-based approximation modeling up to order M.— We consider a Susceptible-Infected-Recovered (SIR) process with higher-order interactions of size $m = 1, \ldots, M$. Each order m has an associated infection rate β_m, which represents the rate at which a susceptible node becomes infected when connected to an m-hyperedge where all m neighbors are infected. The recovery rate is given by μ.

To describe the infection dynamics in a general form, we define $\theta_m(t)$ as the probability that, at time t, a test node u has not been infected through a randomly chosen m-hyperedge from those it belongs to. If the test node u is connected to k_m distinct m-hyperedges, then the probability that u has not been infected through any of them by time t is given by $\theta_m(t)^{k_m}$. Using the probability generating function (PGF) $G_m(x)$ of the m-hyperedge degree distribution, the probability that a randomly chosen node has not received the disease via any m-hyperedge is given by $G_m(\theta_m(t)) = \sum_{k_m=0}^{\infty} P(k_m)\theta_m(t)^{k_m}$. The probability of a node being susceptible at time t is the product of these probabilities across all orders of interaction, which corresponds to the average susceptible population:

$$\langle S(t)\rangle = \prod_{m=1}^{M} G_m(\theta_m(t)) = \prod_{m=1}^{M} \sum_{k_m=0}^{\infty} P_m(k_m)\theta_m(t)^{k_m}. \tag{7}$$

If a test node u is in an m-hyperedge containing s susceptible, i infected, and $m-(s+i)$ recovered neighbors, the probability that u remains uninfected through this m-hyperedge is defined as $\Phi_m^{(s,i)}(t)$. Thus, $\theta_m(t)$ can be decomposed as:

$$\theta_m(t) = \sum_{(s,i)\in\Omega} \Phi_m^{(s,i)}(t), \tag{8}$$

where $\Omega = \{(s,i) \mid 0 \le s+i \le m\}$. For example, $\Phi_5^{(1,3)}(t)$ represents the probability that a test node is in a 5-hyperedge with 1 susceptible, 3 infected, and 1 recovered neighbor, and has not been infected up to time t.

The temporal evolution of $\theta_m(t)$ is governed by:

$$\dot{\theta}_m(t) = -\beta_m \Phi_m^{(0,m)}(t), \tag{9}$$

since infections through an m-hyperedge occur only when all its m neighbors are infected. The evolution of $\Phi_m^{(0,m)}(t)$ depends on transitions between all $\Phi_m^{(s,i)}(t)$ states in Ω. These transitions are influenced by external infections, internal infections, and recoveries, leading to recursive dependencies. The recursive dependencies lead to the variable $\Phi_m^{(m,0)}$, representing the probability that a test node u has not been infected via an m-hyperedge because all its members remain susceptible. To compute $\Phi_m^{(m,0)}$, consider a neighbor v of node u within an m-hyperedge. The degree of v follows the excess distribution $Q_m(k_m) = k_m P(k_m)/\langle k_m\rangle$. The probability that node v has not been infected via any of its other m-hyperedges is $\theta_m^{k_m-1}$, and that it remains susceptible through interactions of any other order n is $\theta_n^{k_n}$, where $Q_n(k_n) = P_n(k_n)$. Combining these factors, the probability that all m nodes in an m-hyperedge to which u belongs are susceptible is:

$$\Phi_m^{(m,0)} = \left(\frac{G_m'(\theta_m)}{\langle k_m\rangle} \prod_{n\neq m} G_n(\theta_n) \right)^m. \tag{10}$$

At the start of the epidemic, $\theta_m(t) \approx \Phi_m^{(m,0)}(t) \approx 1$ for any m. Transitions from $\Phi_m^{(m,0)}$ to $\Phi_m^{(m-1,1)}$ occur due to external infections, where a susceptible neighbor of u becomes infected through another group. The rate of external infections for an m-hyperedge, denoted B_m, can be expressed as:

$$B_m = -\frac{G_m''(\theta_m)\prod_{n\neq m} G_n(\theta_n)\dot{\theta}_m + \sum_{n\neq m} G_m'(\theta_m)G_n'(\theta_n)\prod_{p\neq m,n} G_p(\theta_p)\dot{\theta}_n}{G_m'(\theta_m)\prod_{n\neq m} G_n(\theta_n)}. \tag{11}$$

The probabilities $\Phi_m^{(s,i)}(t)$ are treated as compartments, and the transitions between them are described by a set of differential equations. The rate of change $\dot{\Phi}_m^{(s,i)}$ accounts for eight terms: five decreasing (external infection of susceptible neighbors, internal infection of susceptible neighbors from lower orders and higher orders, internal infection of test node and recovery) and three increasing (infection of a susceptible neighbor or the test node itself, and recovery of an infected neighbor).

Considering these transitions, the differential equation for $\dot{\Phi}_m^{(s,i)}$ is:

$$\begin{aligned}\dot{\Phi}_m^{(s,i)} =& -sB_m\Phi_m^{(s,i)}(t) - \delta^*_{i,0}\sum_{j=1}^{i} s\binom{i}{j}\alpha_{j,m}\beta_j\Phi_m^{(s,i)}(t) - \delta^*_{i,0}\sum_{j=1}^{i}\delta^*_{j,m}\binom{i}{j}\alpha_{j,m}\beta_j\Phi_m^{(s,i)}(t) - \delta_{i,m}\beta_m\Phi_m^{(s,i)} \\ &- \delta_{i,m}\delta^*_{M,m}\sum_{k=m+1}^{M}\sum_{j=1}^{k-1}\binom{k}{j}\alpha_{j,k}\beta_j\Phi_k^{(0,k)} - \mu i\Phi_m^{(s,i)}(t) + \delta^*_{s,m}(s+1)B_m\Phi_m^{(s+1,i-1)} \\ &+ \delta^*_{s+i,m}\mu(i+1)\Phi_m^{(s,i+1)} + \delta^*_{i-1,0}\delta^*_{i,0}\sum_{j=1}^{i-1}(s+1)\binom{i-1}{j}\alpha_{jm}\beta_j\Phi_m^{(s+1,i-1)},\end{aligned} \tag{12}$$

where $\alpha_{i,j}$ is the inter-order overlap between i- and j-hyperedges, $\delta_{i,j}$ represents the Kronecker delta and $\delta^*_{i,j} = (1-\delta_{i,j})$. By leveraging $\alpha_{i,j}$, we are able to to incorporate dynamical correlations arising from the embedding of i- within j-hyperedges, without system closures tailored to specific microscopic configurations.

The system is solved numerically using the following equations:

$$\begin{aligned}\dot{\boldsymbol{\Theta}} &= -\boldsymbol{\beta}\boldsymbol{\Phi}_I, \\ \dot{\boldsymbol{\Phi}}_1 &= \boldsymbol{f}(\boldsymbol{\beta}, \boldsymbol{B}, \boldsymbol{\Phi}_1, \boldsymbol{\Phi}_2 ... \boldsymbol{\Phi}_M), \\ &\vdots \\ \dot{\boldsymbol{\Phi}}_M &= \boldsymbol{f}(\boldsymbol{\beta}, \boldsymbol{B}, \boldsymbol{\Phi}_1, \boldsymbol{\Phi}_2 ... \boldsymbol{\Phi}_M),\end{aligned} \tag{13}$$

where we used the following notations $\boldsymbol{\beta} = \{\beta_1, \beta_2 ... \beta_M\}$, $\boldsymbol{B} = \{B_1, B_2 ... B_M\}$, $\boldsymbol{\Theta} = \{\theta_1, \theta_2 ... \theta_M\}$,$\boldsymbol{\Phi}_I = \{\Phi_1^{(0,1)}, \Phi_2^{(0,2)} ... \Phi_M^{(0,M)}\}$ and $\boldsymbol{\Phi}_m$ represents the set of $\Phi_m^{(s,i)}(t)$ such that $(s,i) \in \Omega$.

Appendix B: Epidemic threshold for $M = 2$.— To derive the epidemic threshold for the GBCM in the case of $M = 2$, we consider the system in Eqs.(4). Here, B_1 and B_2 represent the rates of infection to a susceptible node connected to the test node u through 1-hyperedges and 2-hyperedges, respectively. From Eq. (11), they are defined as:

$$\begin{aligned}B_1 &= -\frac{G''(\theta_1)H(\theta_2)\dot{\theta}_1 + H'(\theta_2)G'(\theta_1)\dot{\theta}_2}{G'(\theta_1)H(\theta_2)}, \\ B_2 &= -\frac{G'(\theta_1)H'(\theta_2)\dot{\theta}_1 + G(\theta_1)H''(\theta_2)\dot{\theta}_2}{G(\theta_1)H'(\theta_2)}.\end{aligned} \tag{14}$$

Furthermore, given the definition in Eq.(10), we obtain $\Phi_1^{(1,0)} = \phi_S = G'(\theta_1)H(\theta_2)/\langle k_1\rangle$ and $\Phi_2^{(2,0)} = \phi_{SS} = (G(\theta_1)H'(\theta_2)/\langle k_2\rangle)^2$. Given that, to assess the stability of the system, we substitute the equations for $\dot{\theta}_1$ and $\dot{\theta}_2$ given by Eqs. (4) and evaluate the Jacobian matrix of the system around the disease-free equilibrium $(\theta_1, \theta_2, \phi_I, \phi_{SI}, \phi_{II}) = (1, 1, 0, 0, 0)$. By considering the free term in the characteristic polynomial of the Jacobian matrix, we derive the epidemic threshold as

$$\lambda_2 = \frac{2\langle k_2\rangle^2\left[\left(\langle k_1\rangle + \alpha\lambda_1\right)\left(\langle k_1\rangle + 2\alpha\lambda_1\right)\left(\langle k_1\rangle^2 - \lambda_1\Delta_1\right) - \Pi_1(\langle k_1\rangle - 1)\langle k_1\rangle^2\lambda_1 + 2\alpha^2\langle k_1\rangle^4\lambda_1^3\right]}{\langle k_1\rangle\left[\langle k_1\rangle^3\langle k_2\rangle - \langle k_1\rangle\langle k_2\rangle\Delta_1\lambda_1 - 2\langle k_1\rangle^2\Delta_2\alpha\lambda_1 + 2\left[\Omega_{1,2} - 2\left(\langle k_1\rangle\Pi_2 + \langle k_2\rangle\Pi_1\right)\right]\alpha\lambda_1^2\right]}, \tag{15}$$

where $\Pi_m = \langle k_m^2\rangle - \langle k_m\rangle = \sum_{k_m} k_m(k_m-1)P(k_m)$ represents the second derivative of the PGF evaluated at $\theta_m(t) = 1$. Additionally, $\Delta_m = \Pi_m - \langle k_m\rangle$ captures the difference between the second and first derivatives of the PGF at $\theta_m(t) = 1$, and $\Omega_{m,n} = \langle k_m^2\rangle\langle k_n^2\rangle - \langle k_m\rangle^2\langle k_n\rangle^2$ [18]. The detailed calculations are provided in [18].